



## Article

# Preparation, Application and Enhancement Dyeing Properties of ZnO Nanoparticles in Silk Fabrics Dyed with Natural Dyes

Haijuan Du <sup>1,\*</sup>, Mengyuan Yue <sup>1,†</sup>, Xin Huang <sup>1</sup>, Gaigai Duan <sup>2</sup> , Zhihui Yang <sup>1</sup>, Weihang Huang <sup>1</sup>, Wenjie Shen <sup>1</sup> and Xiangfeng Yin <sup>1</sup>

<sup>1</sup> College of Textiles, Zhongyuan University of Technology, Zhengzhou 450007, China

<sup>2</sup> Jiangsu Co-Innovation Center of Efficient Processing and Utilization of Forest Resources, International Innovation Center for Forest Chemicals and Materials, College of Materials Science and Engineering, Nanjing Forestry University, Nanjing 210037, China

\* Correspondence: duhaijuan2009@126.com

† These authors contributed equally to this work.

**Abstract:** In this study, ZnO nanoparticles were prepared by a hydrothermal method with varying the reaction times, material ratios and reaction temperatures. The samples were characterized by scanning electron microscopy (SEM), transmission electron microscopy (TEM), X-ray Diffraction (XRD) and Fourier infrared spectroscopy (FTIR). It was shown that the material ratio significantly affected the structure and morphology of the synthesized ZnO nanoparticles, and then the uneven nano-octahedral structure, uniform nano-octahedral structure, nano-tubular structure, and nano-sheet structure could be obtained successively. The synthesized ZnO nanoparticles as mordant were used for the dyeing of silk fabrics with different natural dyes (tea polyphenols and hematoxylin). Moreover, they could improve the dyeing properties and fastness (wash and light) on silk fabrics to a certain extent.

**Keywords:** ZnO nanoparticles; morphology; dyeing properties; fastness; SEM and TEM images; FTIR spectroscopy



**Citation:** Du, H.; Yue, M.; Huang, X.; Duan, G.; Yang, Z.; Huang, W.; Shen, W.; Yin, X. Preparation, Application and Enhancement Dyeing Properties of ZnO Nanoparticles in Silk Fabrics Dyed with Natural Dyes.

*Nanomaterials* **2022**, *12*, 3953.

<https://doi.org/10.3390/nano12223953>

nano12223953

Academic Editors: Andreu Cabot, Giuseppe Cappelletti and Edward Lester

Received: 8 September 2022

Accepted: 4 November 2022

Published: 9 November 2022

**Publisher's Note:** MDPI stays neutral with regard to jurisdictional claims in published maps and institutional affiliations.



**Copyright:** © 2022 by the authors. Licensee MDPI, Basel, Switzerland. This article is an open access article distributed under the terms and conditions of the Creative Commons Attribution (CC BY) license (<https://creativecommons.org/licenses/by/4.0/>).

## 1. Introduction

With the rapid development of nanomaterials, the research and development of nanomaterials has attracted extensive attention from researchers all over the world [1–5]. Nano zinc oxide is favored for its unique physical and chemical properties worldwide [6]. Nano zinc oxide has many advantages, including strong catalytic activity, a small size, a large specific surface area, a lowered environmental impact, and being reusable [7]. Moreover, compared with other metal oxide nanoparticles, ZnO nanoparticles are easy to prepare, as the main advantages of nano zinc oxide are that it is a biocompatible and low-cost material [8,9]. In recent years, nano zinc oxide has shown potential for applications in biopharmaceuticals, optoelectronic devices, ceramic processing, rubber products, textile printing and dyeing, sewage treatment and other industries [10–14]. Over the years, the preparation of nanoparticles has been described using several methods, such as hydrothermal [15,16], microwave-assisted [17,18], sol-gel [19,20], self-assembling [21], and chemical precipitation [22–25]. Based on the advantages of good uniformity of microcrystalline size and significant cost efficiency of industrial production, the hydrothermal method is more preferred by researchers [26,27]. Moreover, nanotechnology can help control particle size to fit functions that can find more applications for its use. For example, nanoparticles are considered excellent candidates as drug-delivery vehicles. In addition, ZnO nanoparticles have also been reported to bring an improvement in the mechanical and antimicrobial property of silk fibers, which can be used as potent surgical suture material [28].

In recent years, with improvements in living standards, green and safe back-to-nature ways have become a pursuit for many people. A renewed international interest has arisen

in natural dyes as they are among the promising options for developing a greener textile dyeing process [29,30]. Natural plant dyes applied to textile dyeing have been reported to confer a variety of health benefits and functionalities on textiles, such as UV protection, antibacterial activity, deodorization, anti-carcinogenicity, and anti-oxygenation [31–34]. However, due to the low affinity between the colorants and the fibers when natural dyes are used in textile dyeing, they cannot be well fixed on the fibers, resulting in poor color fastness of the dyed fabrics [35–37]. Metal salt as mordant in the traditional color fixing process can improve the color fastness of dyed fabrics, but the use of metal salt pollutes water quality and the environment, and the color of dyed fabrics changes greatly. Moreover, a greater number of metal ions on the fabric can cause partial damage to the human body, such as skin allergy and itching [38]. In contrast, reports regarding any negative effects of nano zinc oxide on the dyeing properties and fastness of natural-dye dyed fabrics are rare.

We prepared nano-ZnO with different morphologies by a hydrothermal method. The prepared nano ZnO nanoparticles as mordant have been used to investigate the impact of the dyeing properties and fastness (wash and light) on silk fabric dyeing with natural dyes (tea polyphenols and hematoxylin). Overall, the introduction of new nanomaterials into traditional dyeing and finishing processes was a small innovation. The following focus is to figure out the mechanism of nanomaterials in functional textiles in order to better achieve the desired results [39,40].

## 2. Materials and Methods

### 2.1. Materials and Methods

Sappanwood and tea-leaves were purchased from Shangyuantang Pharmacy in Nanjing City, Jiangsu Province, China. Double crepe silk fabric was purchased from WENSLI, Hangzhou, China. All chemical reactants (zinc acetate, sodium hydroxide and ethanol) were purchased from Sinopharm (Beijing, China) and used without any further purification steps. Absorbance spectra of the staining solution before and after staining were performed using an Agilent CARY 5000 Scan UV-Vis-NIR spectrophotometer (Germany). Morphological characteristics of the ZnO nanomaterials were observed by field emission scanning electron microscopy (Hitachi Regulus 8100, Japan) and transmission electron microscopy (TEM, FEI TALOS F200X 200 kV, Hillsboro, OR, USA). The compositional quality of the synthesized materials was characterized by Fourier transform infrared spectroscopy (TENSOR37, China) in the mid-infrared (400 to 4000  $\text{cm}^{-1}$ ) range. Color strength (K/S) of the dyed samples was tested by a Datacolor measuring and matching instrument (SF600X, China). A sunlight fastness test of the dyed fabrics was performed using a sunlight fastness meter (Q-SUN-B02, China). A soaping test of the dyed fabrics was performed using a soaping machine (SW-24E, China). The crystal structure of the samples was analyzed by X-ray diffraction in angle range (10–80°) with a diffractometer (Rigaku Smartlab).

### 2.2. Colorant Extraction

#### 2.2.1. Hematoxylin

To extract the hematoxylin colorant, sappanwood roots were first washed and dried and then chopped and powdered. Then, we selected fermentation times (48 h), fermentation solvents and extraction solvents (ethanol:water (3:7,  $v/v$ )) to extract plant dyestuff. The extracting solution was filtered and concentrated in a rotary evaporator flask to 1/3 of the original volume. The concentrated dye solution was freeze-dried under low temperature to obtain hematoxylin.

#### 2.2.2. Tea Polyphenols

Powdered tea was soaked in a 2 L mixture solution of alcohol and water in a beaker at a volume ratio of 3:7 for 100 g. The excess alcohol and water were evaporated in a rotary evaporator at 75 °C. The solution was collected in a rotary evaporator flask and dried in a spray dryer at 170 °C for powder production. The dyed solution exhibited the absorbance spectra of the two colorants as shown in Figure 1.

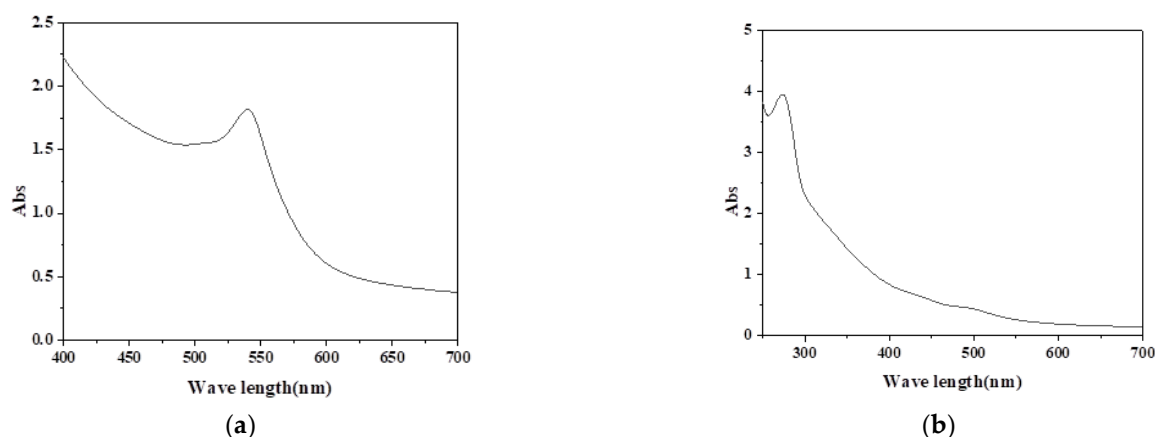


**Figure 1.** The absorbance spectra of hematoxylin (a) and tea polyphenols (b).

### 2.3. Preparation

For hydrothermal growth, a 0.1 mol per liter of zinc acetate ( $\text{Zn}(\text{CH}_3\text{COO})_2 \cdot 2\text{H}_2\text{O}$ ) and 1 mol per liter of sodium hydroxide (NaOH) combined solution was prepared in volumetric flasks to be tested at different hydrothermal reaction times (6 h, 12 h), material ratios of  $\text{Zn}^{2+}$  substance and  $\text{OH}^-$  substance ( $\text{Zn}^{2+}:\text{OH}^-$  (2:1, mol/mol),  $\text{Zn}^{2+}:\text{OH}^-$  (1:1, mol/mol),  $\text{Zn}^{2+}:\text{OH}^-$  (1:2, mol/mol),  $\text{Zn}^{2+}:\text{OH}^-$  (1:4, mol/mol)), and hydrothermal reaction temperatures (100 °C, 130 °C). The preparation conditions for different samples of ZnO nanoparticles are shown in (Table 1).

**Table 1.** Different reaction conditions of ZnO nanoparticles.

Sample	Temperature/°C	Reaction Time/h	Material Ratios ( $\text{Zn}^{2+}:\text{OH}^-$ /(mol/mol))
#1	100	6	2:1
#2	100	6	1:1
#3	100	6	1:2
#4	100	6	1:4
#5	130	6	2:1
#6	130	6	1:1
#7	130	6	1:2
#8	130	6	1:4
#9	100	12	2:1
#10	100	12	1:1
#11	100	12	1:2
#12	100	12	1:4
#13	130	12	2:1
#14	130	12	1:1
#15	130	12	1:2
#16	130	12	1:4

The reaction was placed on a thermostatic magnetic stirrer at a temperature of 50 °C and a speed of 500 r/min. The sodium hydroxide solution was added dropwise to the zinc acetate solution, and the reaction lasted for 30 min. The mixed reacted solutions were transferred to the hydrothermal reactor, which was heated at the set temperature for 0.5 h and then cooled to room temperature at a rate of 10 °C·h<sup>-1</sup>. After the hydrothermal reaction, the resulting product was filtered and rinsed thoroughly with deionized water to remove the excess reactants from its surface. Finally, the samples were dried in an oven at a constant temperature of 60 °C.

#### 2.4. Mordanting and Dyeing

The dyeing process was a simple water bath dyeing under continuous agitation with an alcohol ratio of 1:50, and dye concentration (2% on weight the fabric). The dyeing temperature was 80 °C with a holding time of 60 min, which started from 40 °C with an increase in velocity of 2 °C/min. Holding at 80 °C for 30 min, 0.1 g/L mordant was added and the fabrics continued to be dyed at 80 °C for 30 min. After the dyeing process was completed, the fabrics were washed under running water and dried in a cool place at room temperature.

#### 2.5. Color Measurements

Dyed samples were analyzed by measuring the reflectance curve between 350 and 750 nm with the spectrophotometer with illuminant D<sub>65</sub> at 10 degree observer. For each sample, three measurements at three different sections were made, and the average values were reported. Color strengths (*K/S*) of dyed samples were calculated using the Kubelka-Munk equation:

$$K/S = (1 - R)^2/2R \quad (1)$$

where *R* is the observed reflectance, *K* is the absorption coefficient, and *S* is the light scattering coefficient. In general, the greater the *K/S* value, the deeper the color on the fabric [34,35].

#### 2.6. Determination of Dye Exhaustion

Dye uptake was determined by measuring the absorbance (at the wavelength of maximum absorbance,  $\lambda_{\max} \approx 540$  nm) of the dye bath solution before and after dyeing. According to the Beer-Lambert law, when monochromatic light passes through the solution, the absorbance *D* is proportional to the concentration *C* of the dye in the solution, so there is

$$\% \text{ Dye exhaustion} = \frac{C_0 - C}{C_0} \times 100 = \frac{mD_0 - nD}{mD_0} \times 100 \quad (2)$$

where, *C*<sub>0</sub> is the concentration of the dye in the original dye solution, *C* is the concentration of the dye in the dyeing residue, *D*<sub>0</sub> is the absorbance of the original dye solution diluted *m* times, *D* is the absorbance of the dyeing residue diluted *n* times, *m* is the dilution factor of the original dye solution when measuring the absorbance, and *n* is the dilution factor of the dyeing residue when measuring the absorbance [31].

#### 2.7. Fastness Properties

The wash and light fastness of dyed fabrics were tested in the light of ISO 105-C01, ISO 105-B02, respectively.

### 3. Results

#### 3.1. Structure and Morphology

The different morphologies of ZnO nanoparticles were prepared by the hydrothermal method under different reaction conditions (reaction temperature, reaction time, material ratio), and measured by scanning electron microscopy (SEM) as shown in Figure 2. The SEM results of Figure 2 (#5–#8) show that when the hydrothermal reaction temperature is 130 °C and the reaction time is 6 h, the Zn<sup>2+</sup>:OH<sup>−</sup> material ratio changes (2:1, 1:1, 1:2, 1:4), and then under these conditions, the uneven nano-octahedral structure, uniform nano-octahedral structure, nano-tubular structure, and nano-sheet structure can be obtained successively. This feature indicates that the morphology of ZnO nanoparticles gradually becomes homogeneous as the OH<sup>−</sup> concentration increases. With a further increase in OH<sup>−</sup> concentration, the surface of ZnO nanoparticles is etched on the original octahedral structure, and the central position of ZnO particles is etched to form a nano-tubular structure. When the Zn<sup>2+</sup>:OH<sup>−</sup> material ratio is 1:4, the deposition of zinc oxide is significant

due to the high concentration of  $\text{OH}^-$ , and the longitudinal growth of nano-ZnO crystals is inhibited and a nano-sheet structure is formed.

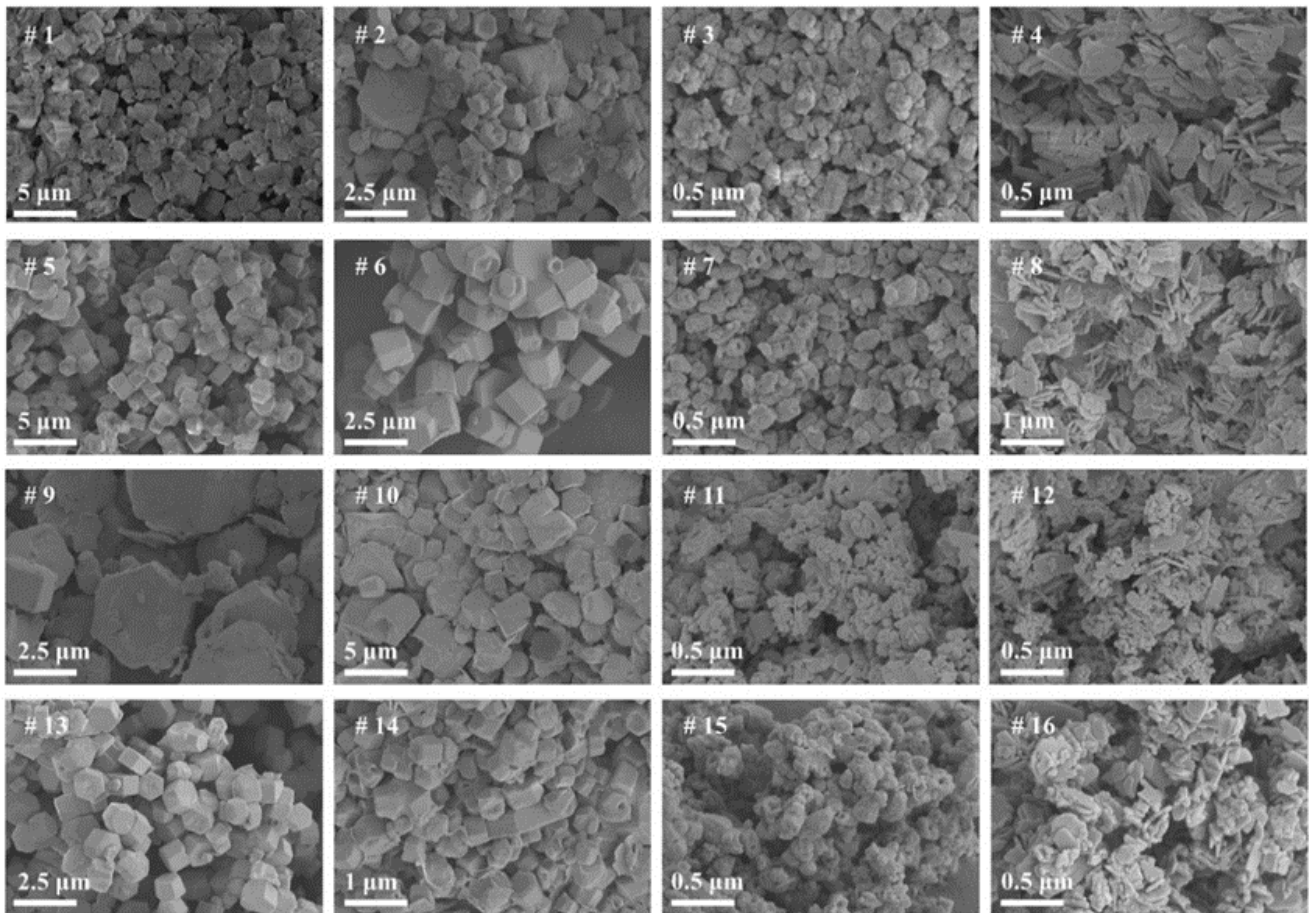


**Figure 2.** SEM images of nano zinc oxide prepared under different reaction conditions (with different reaction temperatures, reaction times and material ratios).

The SEM images in Figure 2 (#1–#4 and #5–#8) show the morphology of ZnO nanoparticles grown at different hydrothermal temperatures (100 °C and 130 °C). It can be seen that the surfaces of nano-ZnO crystals grown at 100 °C are rough and irregular, while the surfaces of nano-ZnO crystals grown at 130 °C are smooth and regular.

The SEM images in Figure 2 (#5–#8 and #13–#16) are the morphology of nano-ZnO crystals grown at different hydrothermal times (6 h and 12 h). With the increase in hydrothermal time, the morphology of nano-ZnO crystals becomes irregular and the nano-surface becomes rough.

The SEM images in Figure 2 (#9–#12 and #13–#16) show the morphology of nano-ZnO crystals grown at different hydrothermal temperatures (100 °C and 130 °C). With the increase in hydrothermal temperature, the size of nanoparticles further increases and the nano-surface becomes smooth.

Further studies on the morphology and structure of the as-synthesized ZnO particles were investigated by TEM (Figure 3). Samples (#5–#8) were selected to test which ones agreed with the SEM results. Moreover, it could be observed that the diameter of the ZnO particles was approximately 500–1500 nm.

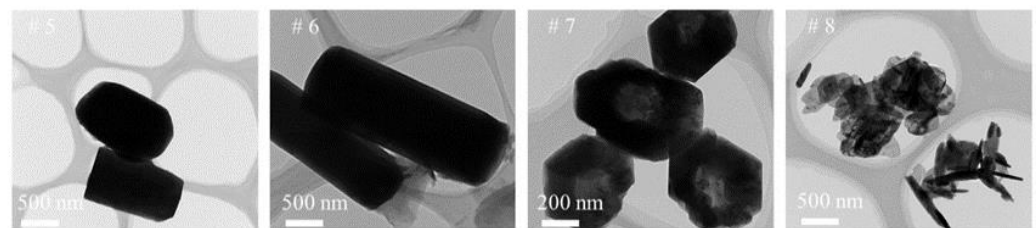


**Figure 3.** TEM images of nano zinc oxide prepared under different reaction conditions (#5–#8 with different material ratios).

### 3.2. X-ray Diffraction (XRD) and FTIR Analysis for the ZnO Nanoparticles

Figure 4a showed the observed XRD patterns of the synthesized ZnO nanoparticles with identified obtained peaks such as (100), (002), (101), (102), (110), (103), (200) and (112) are related to the hexagonal (wurtzite) structure of ZnO. The corresponding XRD peaks of samples 5 and 6 were stronger and sharper, indicating that the samples crystallized well and the average size of particles was bigger than 7 and 8 [41,42].

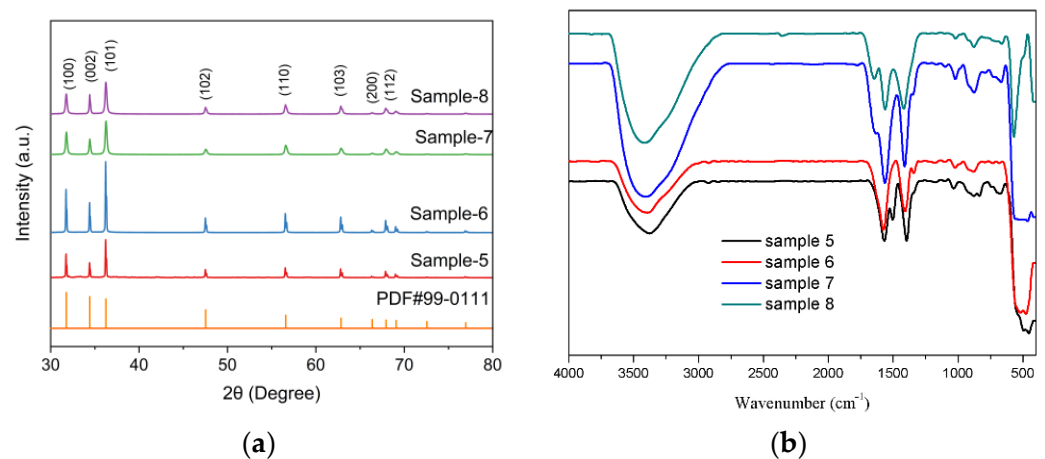


**Figure 4.** The XRD patterns (a) and FTIR spectra (b) for ZnO-NPs.

Figure 4b showed the FTIR spectrum of samples 5–8, which was acquired in the range of 400–4000  $\text{cm}^{-1}$ . The different concentrations of adsorbed water molecules and hydroxyl groups in the sample can be demonstrated by the band strength corresponding to the tensile vibration of the O-H group (3000–3620  $\text{cm}^{-1}$ ). The stretching modes of vibrations in asymmetric and symmetric C=O bonds are observed at 1560 and 1410  $\text{cm}^{-1}$ , respectively. The band at 450  $\text{cm}^{-1}$  is correlated to ZnO [15].

### 3.3. Color Strength of Dyed Fabric with Hematoxylin and Tea Polyphenols

Figure 5 shows the color strength (K/S) of the silk fabrics dyed with hematoxylin and tea polyphenols under the action of different morphology nano-zinc oxide mordants at wavelengths of 350–750 nm. Compared with the unmordanted fabric, the color of the mordant-treated samples became more intense, resulting in greater K/S values. It can be clearly seen that the color strength of nano-ZnO is more intense and the K/S value is greater than that of the original ZnO sample fabric dyed with hematoxylin, and the original color of the dye on the fabric can be well maintained.

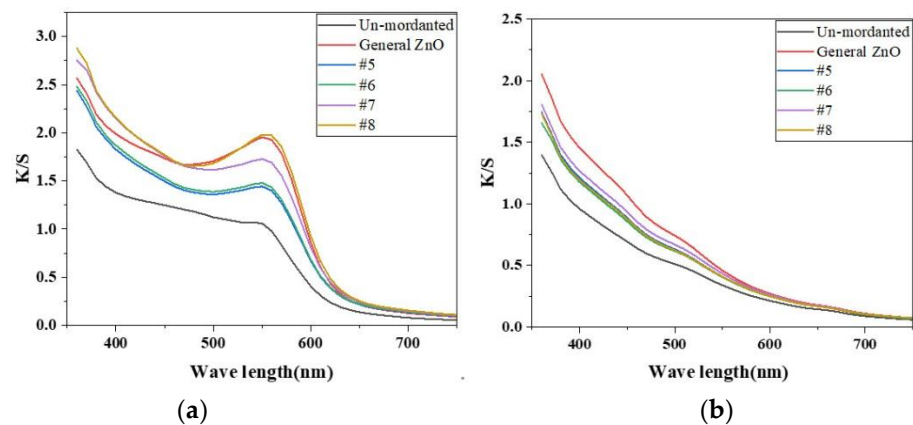


**Figure 5.** The K/S of the silk fabric dyed with hematoxylin (a) and tea polyphenols (b) under the action of different morphology nano-zinc oxide mordants at wavelengths of 350–750 nm.

### 3.4. Dye Exhaustion

The rates of dye exhaustion of hematoxylin and tea polyphenols on silk fabric under the action of different morphology nano-zinc oxide mordants are shown in Figure 6. The addition of mordant greatly increased the dye exhaustion. It was found that the nano-zinc oxide mordants were more helpful in increasing dye exhaustion, followed by ordinary zinc oxide and unmordanted silk fabrics. Compared with ordinary zinc oxide, the rates of dye exhaustion of dyed fabrics with nano zinc oxide are obviously improved. Through the SEM images of nano zinc oxide, it can be concluded that the different rates of dye exhaustion were caused by the morphology of nano zinc oxide, which may be due to the surface area increase effect of the synthesized ZnO nanoparticles. In addition, the rates of dye exhaustion of hematoxylin and tea polyphenols are very different for the more hydroxyl groups of tea polyphenols' structure anchoring onto ZnO nanoparticles.

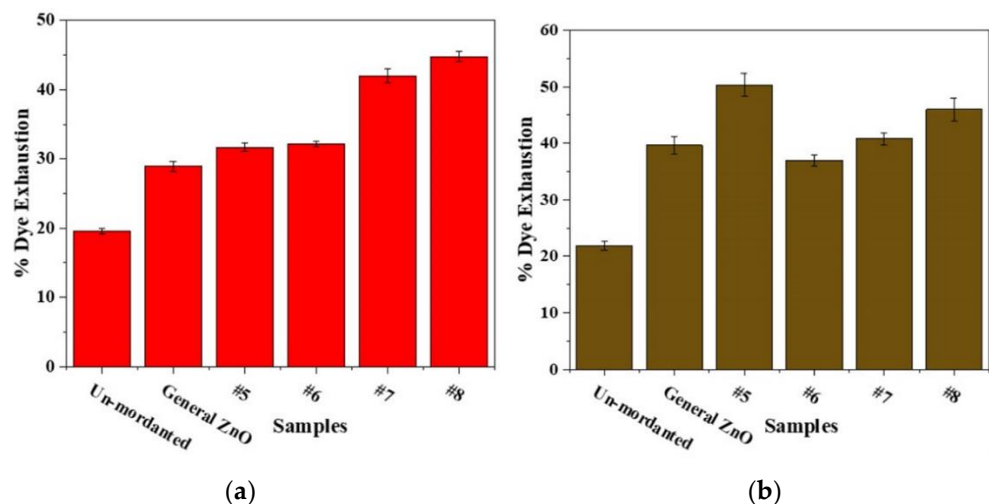


**Figure 6.** The rates of dye exhaustion of hematoxylin (a) and tea polyphenols (b) on silk fabric under the action of different morphology nano-zinc oxide mordants.

### 3.5. Fastness Properties

The fastness (wash and light) of the silk fabrics dyed with hematoxylin under different mordants are shown in (Table 2). It was found that all the dyed fabrics had poor wash and light fastness. Because the molecular structure of hematoxylin dye itself has multiple hydroxyl groups, it has good water solubility, thus leading to the decrease in wash fastness. Under the light condition, the conjugated system of dye itself is damaged by photo-oxidation and fades. The light fastness of fabrics dyed with nano zinc oxide as

mordant are grade 1–2, while that of unmordant fabrics is only grade 1. The wash fastness of fabrics dyed with ZnO nanomaterials as mordant were mostly grade 1–2, among which the washing color fastness of sample 9 was grade 2, while the wash color fastness of fabric dyed with ordinary ZnO mordants was only grade 1.

**Table 2.** Color fastness of silk fabrics dyed with hematoxylin under the action of different mordants.

Substrate	Mordant	Light Fastness	Wash Fastness (Color Change)
Silk	-	1	1–2
	ZnO	1–2	1
	#1	1–2	1–2
	#2	1–2	1–2
	#3	1–2	1–2
	#4	1–2	1–2
	#5	1–2	1–2
	#6	1–2	1–2
	#7	1–2	1–2
	#8	1–2	1
	#9	1–2	2
	#10	1–2	1–2
	#11	1–2	1
	#12	1–2	1–2
	#13	1–2	1–2
	#14	1–2	1–2
#15	1–2	1	
#16	1–2	1	

The fastness (wash and light) of silk fabrics dyed with tea polyphenols under the action of different mordants are shown in (Table 3). The results showed that the light fastness of the fabrics dyed with nano zinc oxide as mordant could reach grade 3, while that of the traditional metal mordant was grade 2–3. The wash fastness of dyed fabrics with nano zinc oxide as mordant were above grade 3–4, among which the wash fastness of dyed fabrics with samples #1, #2, #10 and #12 as mordant could reach grade 4–5, the wash fastness of dyed fabrics with samples #3, #13, #14 and #16 as mordant were grade 4, while the color fastness of dyed samples with ordinary zinc oxide as mordant was grade 3.

**Table 3.** Color fastness of silk fabrics dyed with tea polyphenols under the action of different mordants.

Substrate	Mordant	Light Fastness	Wash Fastness (Color Change)
Silk	-	2–3	3–4
	ZnO	2–3	3
	#1	3	4–5
	#2	3	4–5
	#3	3	4
	#4	3	3
	#5	3	3–4
	#6	3	3–4
	#7	3	3–4
	#8	3	3–4
	#9	3	3
	#10	3	4–5
	#11	3	3–4
	#12	3	4–5
	#13	3	4
	#14	3	4
#15	3	3–4	
#16	3	4	

#### 4. Conclusions

In summary, ZnO nanoparticles were prepared by a simple hydrothermal method. We may draw a conclusion that the surface area increases their effect and the biocompatibility of ZnO nanoparticles as mordant was noteworthy. They can improve the dyeing properties and fastness (wash and light) of hematoxylin and tea polyphenols on silk fabric to a certain extent. In addition, the color of dyed fabrics with ZnO nanoparticles as mordant could be maintained very well compared with the metal mordants. Therefore, this method can be an effective way to enhance the dyeing fastness of natural dyes. However, the K/S of the silk fabrics dyed with hematoxylin and tea polyphenols under the action of different morphology nano-zinc oxide mordants showed no significant improvement compared with ordinary ZnO mordant.

**Author Contributions:** Validation, X.H., G.D., Z.Y. and W.H.; investigation, X.Y. and W.S.; writing—original draft preparation M.Y.; writing—review and editing, H.D. All authors have read and agreed to the published version of the manuscript.

**Funding:** The authors are thankful to the Foundation for University Key Teacher by Henan Province (2021GGJS107). This work was supported by the Foundation for University Key Teacher by Henan Province (2021GGJS107) and 2021 Scientific Research and Entrepreneurial Start-Ups Foundation for the Returned Overseas Chinese Scholars, Henan Province.

**Institutional Review Board Statement:** Not applicable.

**Informed Consent Statement:** Not applicable.

**Data Availability Statement:** The data are included in the main text.

**Conflicts of Interest:** The authors declare no conflict of interest.

#### References

1. Rashidi, L.; Khosravi-Darani, K. The Applications of Nanotechnology in Food Industry. *Crit. Rev. Food Sci. Nutr.* **2011**, *51*, 723–730. [[CrossRef](#)] [[PubMed](#)]
2. Yue, J.; Yu, J.; Jiang, S.; Chen, Y. Biomass carbon materials with porous array structures derived from soybean dregs for effective electromagnetic wave absorption. *Diam. Relat. Mater.* **2022**, *126*, 109054. [[CrossRef](#)]
3. Mahmoud, W.M.M.; Rastogi, T.; Kummerer, K. Application of titanium dioxide nanoparticles as a photocatalyst for the removal of micropollutants such as pharmaceuticals from water. *Curr. Opin. Green Sustain. Chem.* **2017**, *6*, 1–10. [[CrossRef](#)]
4. Yang, J.; Li, H.; He, S.; Du, H.; Liu, K.; Zhang, C.; Jiang, S. Facile Electrodeposition of NiCo<sub>2</sub>O<sub>4</sub> Nanosheets on Porous Carbonized Wood for Wood-Derived Asymmetric Supercapacitors. *Polymers* **2022**, *14*, 2521. [[CrossRef](#)] [[PubMed](#)]
5. Khezri, K.; Saeedi, M.; Dizaj, S.M. Application of nanoparticles in percutaneous delivery of active ingredients in cosmetic preparations. *Biomed. Pharmacother.* **2018**, *106*, 1499–1505. [[CrossRef](#)]
6. Du, J.J.; Zhang, Y.Y.; Guo, R.L.; Meng, F.X.; Gao, Y.C.; Ma, C.; Zhang, H.Z. Harmful effect of nanoparticles on the functions of freshwater ecosystems: Insight into nano ZnO-polluted stream. *Chemosphere* **2019**, *214*, 830–838. [[CrossRef](#)]
7. Prasad, A.R.; Williams, L.; Garvasis, J.; Shamsheera, K.O.; Basheer, M.S.; Kuruvilla, M.; Joseph, A. Applications of phyto-genic ZnO nanoparticles: A review on recent advancements. *J. Mol. Liq.* **2021**, *331*, 115805. [[CrossRef](#)]
8. Kangralkar, M.V.; Manjanna, J.; Momin, N.; Rane, K.S.; Nayaka, G.P.; Kangralkar, V.A. Photocatalytic degradation of hexavalent chromium and different staining dyes by ZnO in aqueous medium under UV light. *Environ. Nanotechnol. Monit. Manag.* **2021**, *16*, 100508. [[CrossRef](#)]
9. Zhang, Y.; Wei, L.; Lu, L.; Gan, L.; Pan, M. Adsorption-photocatalytic properties of cellulose nanocrystal supported ZnO nanocomposites. *J. For. Eng.* **2020**, *5*, 29–35.
10. Jin, S.E.; Jin, H.E. Synthesis, Characterization, and Three-Dimensional Structure Generation of Zinc Oxide-Based Nanomedicine for Biomedical Applications. *Pharmaceutics* **2019**, *11*, 575. [[CrossRef](#)]
11. Feng, Y.X.; Yu, H.Y.; Li, H.J.; Qian, D.J. Interfacial self-assembly of nanoZnO@multiporphyrin array hybrids as binary light-sensitizers for photocurrent generation and photocatalytic degradation of organic pollutants. *Appl. Surf. Sci.* **2020**, *521*, 146465. [[CrossRef](#)]
12. Pascariu, P.; Homocianu, M. ZnO-based ceramic nanofibers: Preparation, properties and applications. *Ceram. Int.* **2019**, *45*, 11158–11173. [[CrossRef](#)]
13. Beura, R.; Pachaiappan, R.; Paramasivam, T. Photocatalytic degradation studies of organic dyes over novel Ag-loaded ZnO-graphene hybrid nanocomposites. *J. Phys. Chem. Solids* **2021**, *148*, 109689. [[CrossRef](#)]
14. Mohammed, R.; Ali, M.; Gomaa, E.; Mohsen, M. Green ZnO nanorod material for dye degradation and detoxification of pharmaceutical wastes in water. *J. Environ. Chem. Eng.* **2020**, *8*, 104295. [[CrossRef](#)]

15. Zandi, S.; Kameli, P.; Salamati, H.; Ahmadvand, H.; Hakimi, M. Microstructure and optical properties of ZnO nanoparticles prepared by a simple method. *Phys. B* **2011**, *406*, 3215–3218. [[CrossRef](#)]
16. Jian, S.J.; Ma, X.F.; Wang, Q.M.; Wu, J.L.; Wang, Y.F.; Jiang, S.H.; Xu, W.H.; Yang, W.S. Hierarchical porous Co<sub>3</sub>O<sub>4</sub> nanocages with elaborate microstructures derived from ZIF-67 toward lithium storage. *Vacuum* **2021**, *184*, 109879. [[CrossRef](#)]
17. Filip, A.; Musat, V.; Tigau, N.; Polosan, S.; Pimentel, A.; Ferreira, S.; Gomes, D.; Calmeiro, T.; Martins, R.; Fortunato, E. ZnO nanostructures grown on ITO coated glass substrate by hybrid microwave-assisted hydrothermal method. *Optik* **2020**, *208*, 164372. [[CrossRef](#)]
18. Zheng, J.J.; Hanshe, M.; Sun, Z.X.; Chen, Y.M.; Jiang, S.H.; Zhang, Y.X.; Cao, Y.X.; Li, X.P.; Shiju, E. From waste to wealth: Crumb rubber@carbon nanotube/Fe<sub>3</sub>O<sub>4</sub> composites towards highly effective electromagnetic microwave absorption with wide bandwidth. *Diam. Relat. Mater.* **2022**, *126*, 109089. [[CrossRef](#)]
19. Abdullah, K.A.; Awad, S.; Zaraket, J.; Salame, C. Synthesis of ZnO Nanopowders by Using Sol-Gel and Studying Their Structural and Electrical Properties at Different Temperature. *Energy Procedia* **2017**, *119*, 565–570. [[CrossRef](#)]
20. Guo, H.; Jiang, S.; Zeng, G.; Zhou, W. Microstructure and electrochemical performances of TiO<sub>2</sub>-coated Mg-Zr co-doped NCM as cathode materials for lithium-ion batteries with high power and long circular life. *New J. Chem.* **2021**, *45*, 19446–19455.
21. Li, Y.; Tong, S.; Li, R.; Dai, L.; Si, C. Preparation and properties of Fe/lignin nanoparticle composite paper. *J. For. Eng.* **2021**, *6*, 123–129.
22. Adam, R.E.; Pozina, G.; Willander, M.; Nur, O. Synthesis of ZnO nanoparticles by co-precipitation method for solar driven photodegradation of Congo red dye at different pH. *Photonics Nanostruct.* **2018**, *32*, 11–18. [[CrossRef](#)]
23. Xia, H.; An, J.; Zhang, W.; Ge, C.; Zuo, S. Effect of the metal-support interaction on catalytic oxidation performances of HMF on Ag nanoparticles. *J. For. Eng.* **2020**, *5*, 88–93.
24. Chen, X.; Wei, M.; Jiang, S.; Förster, S. Two growth mechanisms of thiol-capped gold nanoparticles controlled by ligand chemistry. *Langmuir* **2019**, *35*, 12130–12138. [[CrossRef](#)] [[PubMed](#)]
25. Zhang, C.; Li, Z.; Fang, Y.; Jiang, S.; Wang, M.; Zhang, G. MnO<sub>2</sub> mediated sequential oxidation/olefination of alkyl-substituted heteroarenes with alcohols. *Tetrahedron* **2020**, *76*, 130968. [[CrossRef](#)]
26. Win, T.T.; Maung, Y.M.; Soe, K.K.K. Characterization of Nano-sized ZnO Electrodes with Curcumin-derived Natural Dye Extract for DSSC Application. *Am. J. Mater. Sci. Technol.* **2012**, *1*, 28–33. [[CrossRef](#)]
27. Cunha, D.M.; Ito, N.M.; Xavier, A.M.; Arantes, J.T.; Souza, F.L. Zinc oxide flower-like synthesized under hydrothermal conditions. *Thin Solid Films* **2013**, *537*, 97–101. [[CrossRef](#)]
28. Shubha, P.; Gowda, M.L.; Namratha, K.; Shyamsunder, S.; Manjunatha, H.B.; Byrappa, K. Ex-situ fabrication of ZnO nanoparticles coated silk fiber for surgical applications. *Mater. Chem. Phys.* **2019**, *231*, 21. [[CrossRef](#)]
29. Du, H.J.; Cheng, J.; Wang, M.H.; Tian, M.C.; Yang, X.M.; Wang, Q. Red dye extracted sappan wood waste derived activated carbons characterization and dye adsorption properties. *Diam. Relat. Mater.* **2022**, *102*, 107646. [[CrossRef](#)]
30. Zhang, G.; Liang, Q.; Yang, W.; Jiang, S.; Wang, Z.; Zhang, C.; Zhang, G. One Pot Synthesis of 1, 2-Disubstituted Ethanones by Base-Mediated Reductive Homocoupling of Aldehydes. *Adv. Synth. Catal.* **2020**, *364*, 2951–2956. [[CrossRef](#)]
31. Zhou, Q.; Rather, L.J.; Ali, A.; Wang, W.C.; Zhang, Y.Y.; Haque, Q.M.R.; Li, Q. Environmental friendly bioactive finishing of wool textiles using the tannin-rich extracts of Chinese tallow (*Sapium sebiferum* L.) waste/fallen leaves. *Dye. Pigment.* **2020**, *176*, 108230. [[CrossRef](#)]
32. Phan, K.; Raes, K.; Van Speybroeck, V.; Roosen, M.; De Clerck, K.; De Meester, S. Non-food applications of natural dyes extracted from agro-food residues: A critical review. *J. Clean. Prod.* **2021**, *301*, 126920. [[CrossRef](#)]
33. Gong, K.; Pan, Y.; Rather, L.J.; Wang, W.C.; Zhou, Q.; Zhang, T.H.; Li, Q. Natural pigment during flora leaf senescence and its application in dyeing and UV protection finish of silk and wool—A case study of Cinnamomum Camphora. *Dye. Pigment.* **2019**, *166*, 114–121. [[CrossRef](#)]
34. Du, H.J.; Wang, Q.; Tian, M.C.; Yang, X.M. Simple crystallization approach for enhancing function of plant-based madder dye and performance of dyed fabric. *Heliyon* **2019**, *5*, e02232. [[CrossRef](#)]
35. Rehman, A.; Ahmad, A.; Hameed, A.; Kiran, S.; Farooq, T. Green dyeing of modified cotton fabric with *Acalypha wilkesiana* leave extracts. *Sustain. Chem. Pharm.* **2021**, *21*, 100432. [[CrossRef](#)]
36. Phan, K.; Van Den Broeck, E.; Van Speybroeck, V.; De Clerck, K.; Raes, K.; De Meester, S. The potential of anthocyanins from blueberries as a natural dye for cotton: A combined experimental and theoretical study. *Dye. Pigment.* **2020**, *176*, 108180. [[CrossRef](#)]
37. Patel, B.; Kanade, P. Iron-tannin complex effect on coloration and functional properties of silk fabric. *Sustain. Chem. Pharm.* **2021**, *22*, 100490. [[CrossRef](#)]
38. Shahidul, I.; Mohammad, F. Natural Colorants in the Presence of Anchors So-Called Mordants as Promising Coloring and Antimicrobial Agents for Textile Materials. *ACS Sustain. Chem. Eng.* **2015**, *3*, 2361–2375. [[CrossRef](#)]
39. Avazpour, S.; Karimi, L.; Zohoori, S. Simultaneous coloration and functional finishing of cotton fabric using Ag/ZnO nanocomposite. *Color. Technol.* **2017**, *133*, 423–430. [[CrossRef](#)]
40. Eskani, I.N.; Haerudin, A.; Setiawan, J.; Lestari, D.W.; Isnaini; Astuti, W. Modification of cotton fabric by ZnO nanoparticles for producing an antibacterial natural dyed batik. *IOP Conf. Ser. Earth Environ. Sci.* **2020**, *462*, 012031. [[CrossRef](#)]

41. Mohamed, M.; Sedky, A.; Kassem, M.A. Gradual growth of ZnO nanoparticles from globules-like to nanorods-like shapes: Effect of annealing temperature. *Optik* **2022**, *265*, 169559. [[CrossRef](#)]
42. Alshraiedeh, N.H.; Ammar, O.F.; Masadeh, M.M.; Alzoubi, K.H.; Al-Fandi, M.G.; Oweis, R.J.; Alsharedeh, R.H.; Alabedr, R.A.; Hayajneh, R.H. Comparative Study of Antibacterial Activity of Different ZnO Nanoparticles, Nanoflowers, and Nanoflakes. *Curr. Nanosci.* **2022**, *18*, 758–765. [[CrossRef](#)]